Porous Alumina Membranes

Dressing in Layers: Layering Surface Functionalities in Nanoporous Aluminum Oxide Membranes**

Abdul Mutalib Md Jani, Ivan M. Kempson, Dusan Losic,* and Nicolas H. Voelcker*

Enhanced control over the surface properties of porous materials is of great interest owing to applications as diverse as the detection of chemical and biological species, molecular separation, drug delivery, and catalysis.[1–3] Recent research has made inroads into this issue, devising experimental strategies towards surface manipulation in porous materials.[4–7] However, the increasingly stringent device requirements for advanced applications, such as energy storage, controlled release, biochemical gates, nanoreactors, sorption, and high-performance molecular transport and separation, demand the development of multiphasic, responsive, and multifunctional materials.[8–10]

Self-organized nanoporous anodic aluminum oxide (AAO) membranes prepared by electrochemical anodization have become popular materials, attractive for their high surface area (up to $250 \, m^2 g^{-1}$), high porosity (10^{10} pores cm^{-2}), highly ordered and monodisperse pores, tunable thickness and pore dimensions, excellent chemical, thermal, and mechanical stability, biocompatibility, and inexpensive fabrication.[11] A considerable number of studies have been devoted to the development of AAO membranes with complex pore geometries in order to improve the membrane properties for applications in molecular separation[12] and to enable the template synthesis[13] of sophisticated nanostructures with novel architectures[14] and unique optical,[15] magnetic,[16] energy-storage,[17] and electrical properties.[18,19] Membranes with branched, multilayered, and modulated pore structures have been generated by precise and temporal control over the anodization conditions.[20] In contrast, control at a similar level of complexity over the surface inside the pores of AAO membrane is currently lacking, despite the fact that the functionality on the pore surface is a key determinant for device performance. In particular, the selectivity and efficiency of molecular transport and separation through AAO membranes are not only effectively modulated by changing the size,[21] but also by the charge[22] and polarity[23] of the porous layer and the engineered affinity towards the species of interest.[24] Several surface-modification techniques have been applied to AAO membranes including silanization,[25] formation of self-assembled monolayers,[26] grafting of polymer brushes,[27] plasma processing,[28] sol–gel modification,[29,30] metal deposition (chemical vapor deposition, electroless and pulse electrochemical plating),[31] and quantum-dot adsorption.[32]

However, multifunctional and multilayered surface modification has not been demonstrated until our recent work in which we fabricated AAO membranes with distinctly different internal and external surface functionalities.[33] This study provided a glimpse of the opportunities for controlling the surface properties in porous materials but stopped short of demonstrating truly multilayered surface modifications, tunability, and functional properties. Here, we describe AAO membranes having pores with spatially controlled multilayered surface functionalities, selected self-assembly of gold nanoparticles on amino-functionalized layers, and selective membrane transport. Membranes with layered surface functionalities inside the pore channel were prepared by a series of anodization and silanization cycles with pentafluorophenyldimethylpropylchlorosilane (PFPTES), 3-aminopropyltriethoxysilane (APTES), and N-triethoxysilylpropyl-O-polyethyleneoxide urethane (PEGS), respectively, achieving a range of functionalities and wettabilities. The fabrication approach is shown schematically in Scheme 1. Typically, at least three anodization steps were used. The first anodization was carried out on electropolished aluminum foil for 3 h using a constant voltage of 40 V at a temperature of 1°C in 0.3 M aqueous oxalic acid ($C_2H_2O_4$). Afterwards, the sacrificial layer was removed by treatment with phosphoric acid/chromium trioxide solution to generate a textured concave pattern on the Al surface, which acted as a template for the subsequent pore formation during the second anodization. Upon completion of this step, the generated porous layer was treated with the first silane. The following third anodization was then performed to generate a virgin porous layer below the first silanized porous layer. We found that silanized surfaces were chemically inert and mechanically stable under anodization conditions. The newly generated pore surfaces were then

[*] A. M. M. Jani, Prof. Dr. N. H. Voelcker
School of Chemical and Physical Sciences
Flinders University
Bedford Park 5042 SA (Australia)
Fax: (+61) 8-8201-2905
E-mail: nico.voelcker@flinders.edu.au
Homepage: http://www.voelckerlab.com

A. M. M. Jani
Universiti Teknologi Mara (UiTM)
40450 Shah Alam, Selangor Darul Ehsan (Malaysia)

Dr. I. M. Kempson
Institute of Physics, Academia Sinica
128 Academia Road, Section 2, Nankang, Taipei 115 (Taiwan)

Dr. D. Losic
Ian Wark Research Institute, University of South Australia
Mawson Lake Campus, Mawson Lake 5035 SA (Australia)

Supporting information for this article (including experimental details of the materials and fabrication methods) is available on the WWW under http://dx.doi.org/10.1002/anie.201002504.
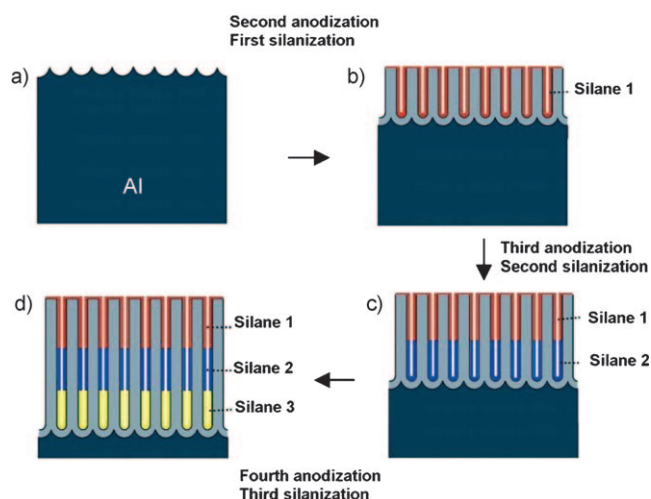
Scheme 1. Schematic diagram of the methods for fabricating an AAO membrane with three different layers displaying distinct chemical functionalities.

Figure 1. a) Cross-sectional measurements of the thickness of a PFPTES-coated layer on the top of a bilayered membrane (APTES coating at the bottom) demonstrating control over the thickness of the top layer by varying the anodization time. b) Fluorescence microscopy image of the cross-section of a freestanding layered AAO membrane with an APTES coating on the top and a PFPTES coating at the bottom of the membrane after reaction with FITC dye. Scale bar = 20 μm. c) Schematic of an AAO membrane with the surface functionalities of (b).

functionalized with a second silane. These steps may be repeated to form additional silane layers, and we have produced membranes with up to five layers. In this work, we show examples with two and three silane layers and different functional groups, length, and orientation.

Once the assembly of the multilayered structure was completed, a freestanding membrane can be prepared by dissolution of the remaining Al substrate, followed by pore opening at the membrane bottom with phosphoric acid (see Scheme S1 in the Supporting Information). We first prepared bilayered nanoporous AAO membranes with a different ratio of thickness between the upper and lower layers where the upper and lower layer were functionalized with the hydrophobic silane PFPTES and the amino-functional silane APTES, respectively (see Figure S1a,b in the Supporting Information). The total thickness of the membrane was held constant in this experiment. Cross-sectional SEM images did not show significant contrast between the two layers with different surface functionality (see Figure S2b in the Supporting Information). We therefore used the fluorescent probe fluorescein isothiocyanate (FITC), which was expected to selectively bind to the amino-functional layer. A cross-sectional fluorescence microscopy image of the bilayered membrane is shown in Figure S2a in the Supporting Information. A strongly fluorescing lower layer can be clearly distinguished from a weakly fluorescing upper layer.

The thickness of the PFPTES layer in the bilayered membrane increased with anodization time (Figure 1a and Figure S2a in the Supporting Information). The method of functionalization described here hence allows control of the thickness of the layers of the desired chemical functionalities. Furthermore, these results show that attachment of APTES to the PFPTES-coated upper layer is minimal (Figure S2a in the Supporting Information). Corroborating the above findings, energy-dispersive X-ray spectroscopy (EDX) analysis of the bilayered membrane showed the presence of silicon, carbon, fluorine, and chlorine elements in the PFPTES layer, confirming that the PFPTES was still intact after being
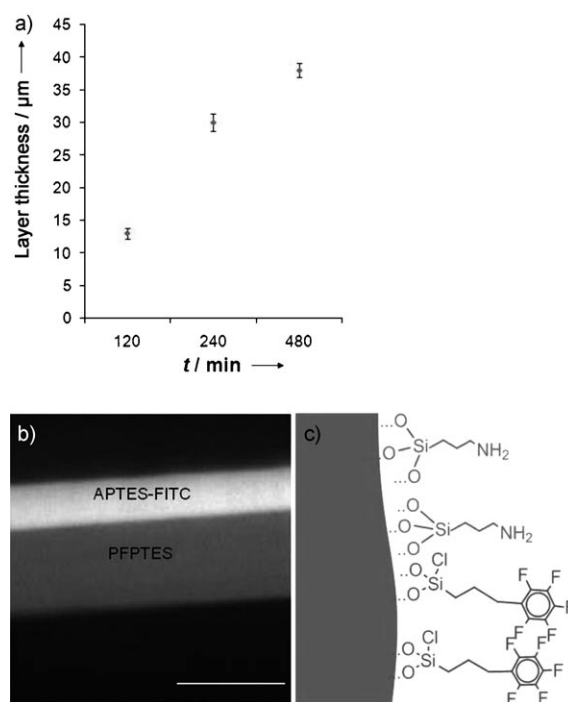
subjected to the anodization conditions. Likewise, the lower layer showed the expected silica and nitrogen peaks for an APTES coating (Figure S3 in the Supporting Information). We next changed the silanization sequence by functionalizing the upper part of the membrane with APTES and the lower segment with PFPTES. Figure 1b shows a cross-sectional fluorescence microscopy image of a freestanding bilayered AAO membrane functionalized with APTES and PFPTES after incubation with FITC dye solution. Once again, we observed that dye attachment was restricted to the APTES-functionalized upper part of the membrane. The lower part of the membrane fluoresced at only 20% of the signal intensity of the upper layer, showing that physisorption of the dye to the lower part of the membrane was successfully blocked by the PFPTES coating.

Furthermore, each of the deposited layers was distinguishable by time-of-flight secondary-ion mass spectrometry (TOF-SIMS) imaging. Exemplar negative-ion images of a membrane cross-section are shown in Figure 2 for a bilayered membrane with a PFPTES-coated upper layer and an APTES-coated lower layer. The total ion yield image (TIY$^-$) reveals the total thickness of the membrane. The thicknesses of layers generating intense F$^-$ and N$^-$ ion signals, on the other hand, correlate with the membrane's PFPTES- and APTES-coated layers, respectively. Line scans across this region are shown in Figure S4 in the Supporting Information. The surface sensitivity of the TOF-SIMS technique enables
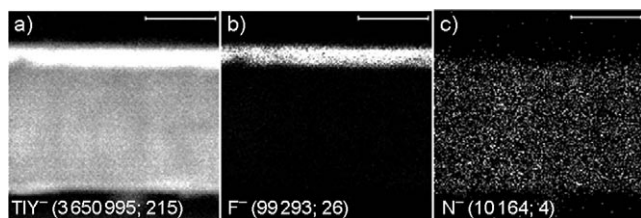
Figure 2. Cross-sectional TOF-SIMS negative-ion images. a) Total ion yield (TIY⁻) image, b) F⁻ and c) N⁻ fragment ion maps. The numbers in parentheses indicate total ion counts and maximum counts per pixel. Scale bar = 10 μm.

clear distinction of chemical layer boundaries, minimizing the distortion arising from depth effects (Figure 2).

Membranes with three different surface functionalities were also prepared. Here, we applied APTES on the top layer, PFPTES on the central, and again APTES on the bottom layer of the membrane (Figure 3 a). Figure 3 b shows a
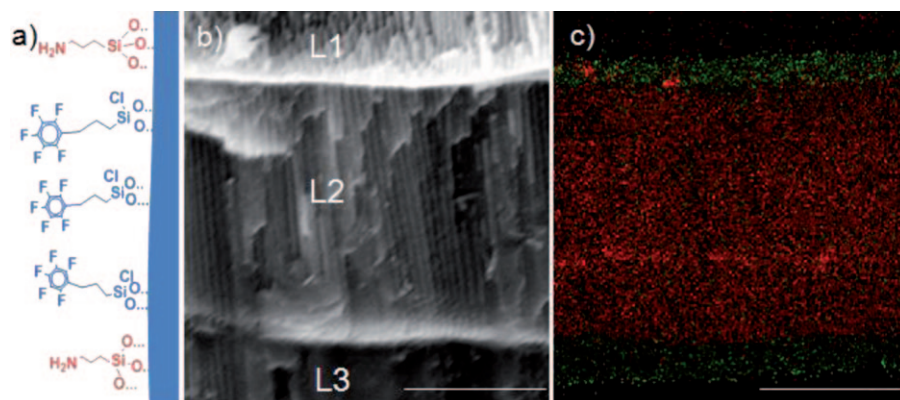

Figure 3. a) Schematic of the three layers of functional groups in the nanoporous AAO membrane. b) Cross-sectional SEM image and c) TOF-SIMS negative-ion image (N⁻ in green and F⁻ in red). Scale bar = 10 μm.

SEM image of such a membrane with three layers of surface modification. The cross-sectional TOF-SIMS image in Figure 3 c shows a two-color map of negative ions where N⁻ fragments are shown in green and F⁻ fragments in red, differentiating APTES- (top and bottom) and PFPTES-functionalized regions (center). The TIY⁻ image of the three-layered membrane is in Figure S5 in the Supporting Information. A membrane containing three layers of surface modifications with another combination of silanes was also fabricated using PFPTES for the top layer of the membrane, APTES for the center, and 3-isocyanatopropyltriethoxysilane for the bottom layer of the membrane. EDX spectra of each layer featured elemental peaks that were consistent with the

expected elemental signatures for the three different silanes (Figure S6 in the Supporting Information).

Confocal microscopy was used as an additional characterization tool for the multilayered membrane. Here, we fabricated a three-layered membrane (PFPTES-APTES-PFPTES) and immobilized FITC to the APTES-functionalized region at the center of the membrane. Figure 4 a,b shows a series of confocal images obtained at regular intervals along the vertical axis of the membrane and an optical section. The thickness of the membrane was measured in reflectance mode. As expected, only the central layer shows strong fluorescence. A plot of the cross-sectional fluorescence intensity signal versus depth is shown in Figure S7 in the Supporting Information.

To illustrate the ability of AAO membranes with layered surface functionalities to separate molecules based on their chemical properties, we fabricated a membrane with two layers and a sharp contrast of hydrophobicity using PFPTES and PEGS in order to tune wettability and chemical selectivity of the membrane towards solutes of different polarity. We produced membranes differing in the ratio of the thickness of PFPTES- and PEGS-coated layers, with 3:1, 1:1, and 1:3 layer thickness ratios of PFPTES and PEGS. The transport and molecular selectivity characteristics of these bilayered AAO membranes were investigated using two different dyes as model compounds with different hydrophobicity and similar molecular size: pinacyanol chloride (PCN) and Rose Bengal (RB). Figure 5 shows the amount of dye in the permeate cell as a function of time for the 3:1 and 1:3 PFPTES/PEGS membranes. In the case of the 3:1 PFPTES/PEGS membrane (Figure 5 a), transport of the hydrophobic dye (PCN, blue line) was faster than that of the hydrophilic dye (RB, red line) by a factor of 3.
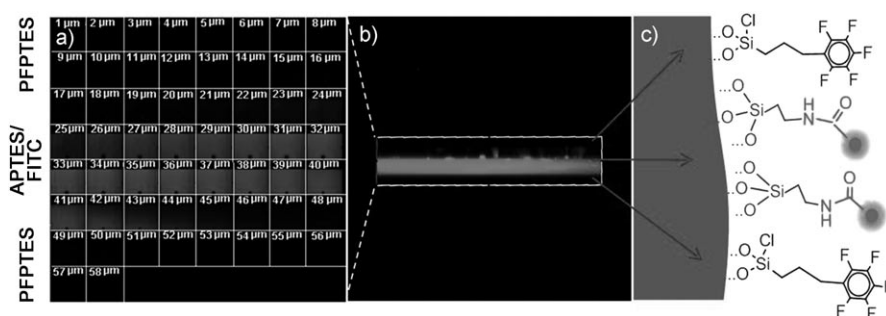

Figure 4. a) Confocal fluorescence microscopy images of three-layered (PFPTES-APTES-PFPTES) AAO membrane along the vertical axis (every 1 μm) from the top to the bottom surface. b) Reconstructed two-dimensional image of the membrane. c) Schematic of the membrane having three layers of surface modifications illustrating FITC immobilization on the central, APTES-functionalized part of the membrane.
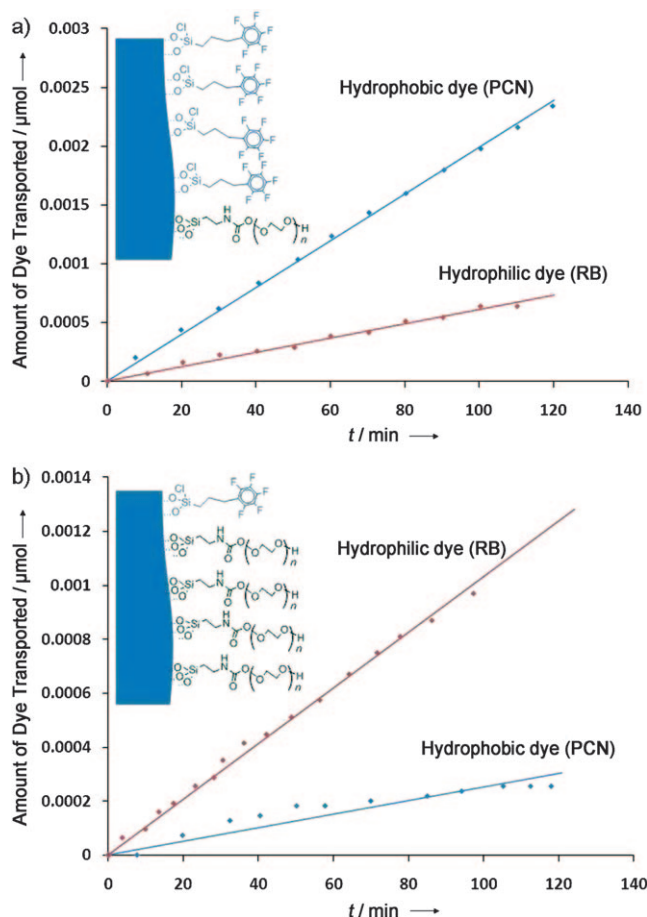
Figure 5. Studies of transport through a bilayered AAO membrane with mixed hydrophobic and hydrophilic character. a) Comparison of transport rate of hydrophobic dye (PCN) and hydrophilic dye (RB) through a bilayered membrane with a 3:1 PFPTES/PEGS layer thickness ratio. b) Transport of RB and PCN through a layered membrane with a 1:3 PFPTES/PEGS layer thickness ratio.

Next, we switched to a membrane with a layer thickness ratio of 1:3 PFPTES/PEGS. This led to a conspicuous change in transport rates for both dyes, as shown in Figure 5b. The flux of hydrophilic dye (RB) now was faster than hydrophobic dye (PCN) by a factor of 3.3. Using a membrane with 1:1 ratio of PFPTES/PEGS, we observed similar transport rates for both dyes (Figure S8 in the Supporting Information). These results effectively demonstrate control over molecular transport and molecular selectivity through AAO membranes with layered surface functionalities inside the pore channels. In our case, it is evident that the diffusion of dye molecules in pores is hindered during the transport of hydrophobic dyes within a hydrophilic layer and hydrophilic dyes within a hydrophobic layer. The diffusional hindrance in pores can be explained by two mechanisms. First, the mobility of the molecule is smaller because of viscous retardation caused by the pore wall, and second, perhaps more important, molecules can be excluded from regions near the pore wall because of their surface properties. In the case of a hydrophobic permeant species (PCN), our results show that molecules are preferentially partitioned into and transported faster through membrane pores containing a thicker hydrophobic (PFPTES) segment

than the more hydrophilic dye RB (Figure 5a). This is the result of an increased hydrodynamic coupling of the PCN with the PFPTES-modified layers, enhancing the diffusion of this dye from the feed cell. In contrast, transport of the more hydrophilic RB will be significantly hindered in the PFPTES layer as result of reduced partitioning of RB into this hydrophobic layer. Membranes with a thicker hydrophilic layer (PEGS) compared to PFPTES (1:3 PFPTES/PEGS layer thickness ratio), preferentially transported RB since partitioning of PCN into this membrane is highly unfavorable (Figure 5b). However, transport of RB through this membrane was only half as fast as transport of PCN through the 3:1 PFPTES/PEGS membrane, indicating that the partitioning effect in a polar environment is more effective for the hydrophobic dye.

Our approach also has the potential to interface other types of nanomaterials such as gold nanoparticles with layers of defined surface functionalization inside the pores of AAO membranes. In order to effectively interface gold nanoparticles with AAO membranes with multilayered surface functionalities, we covalently attached carboxylated gold nanoparticles (16 nm diameter) on the APTES-functionalized top layer of an APTES-PFPTES bilayered AAO membrane using carbodiimide coupling chemistry as shown in Figure S9 in the Supporting Information. Figure 6a depicts
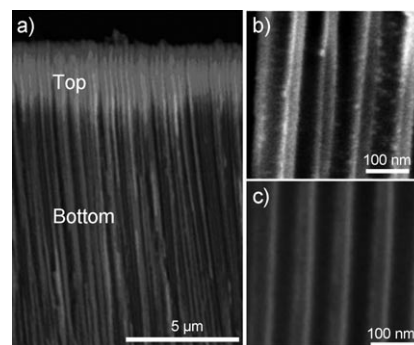

Figure 6. a) Cross-sectional SEM image of a bilayered AAO membrane with an APTES-functionalized top layer and a PFPTES-functionalized bottom layer after coupling of carboxyl-terminal gold nanoparticles. Scale bar = 5 μm. High-resolution SEM image of APTES layer (b) and PFPTES layer (c). Scale bars = 100 nm.

the cross-sectional SEM image of an AAO membrane after the immobilization of gold nanoparticles. A bright top layer can be distinguished in the SEM image from a dark bottom layer. The brightness of the upper layer is consistent with attachment of the gold nanoparticles on the APTES layer since gold nanoparticles are known to give strong secondary electron yields.[34] The high-resolution SEM image recorded on this spot showed gold nanoparticles were selectively bound on amino-functional layer (Figure 6b) and in contrast, no gold nanoparticles were observed attached to the PFPTES layer (Figure 6c). Furthermore, EDX validated this interpretation, since an Au peak was present in an EDX spectrum taken at a spot in the center of the upper layer but not in the lower layer (Figure S10 in the Supporting Information). The transmission FTIR spectra showed characteristic carboxylic acid and

amide peaks on the upper membrane surface at 1400–1420 and 1650 cm^{-1}, respectively, after immobilization of the gold nanoparticles (Figure S11 in the Supporting Information).

In summary, we have developed a facile yet powerful technique for spatially controlling the surface modifications inside the pores of AAO membranes. We demonstrated multilayered surface modifications by applying several anodization and silanization cycles. The thickness of the generated chemical layers was controlled by tuning the anodization time. Chemical contrast, on the other hand, was engineered by judicious choice of silane compounds. Layered membranes produced by this technique were chemically robust and mechanically stable, and showed selectivity towards the transport of small molecular compounds, rendering these multifunctional membranes useful components of future and advanced sensing, separation, filtration, or controlled-release devices. Finally, selective attachment of gold nanoparticles to individual layers exemplifies the potential of these composite nanostructured materials as catalytically active or stimuli-sensitive membranes.[35]

[1] M. Miyazaki, H. Maeda, *Trends Biotechnol.* **2006**, *24*, 463.

[2] J. Fu, P. Mao, J. Han, *Trends Biotechnol.* **2008**, *26*, 311.

[3] P. W. Bohn, *Annu. Rev. Anal. Chem.* **2009**, *2*, 279.

[4] M. E. Davis, *Nature* **2002**, *417*, 813.

[5] A. Stein, *Adv. Mater.* **2003**, *15*, 763.

[6] F. Schüth, W. Schmidt, *Adv. Eng. Mater.* **2002**, *4*, 269.

[7] K. A. Kilian, T. Böcking, K. Gaus, J. J. Gooding, *Angew. Chem.* **2008**, *120*, 2737; *Angew. Chem. Int. Ed.* **2008**, *47*, 2697.

[8] S. J. Son, X. Bai, A. Nan, H. Ghandehari, S. B. Lee, *J. Controlled Release* **2006**, *114*, 143.

[9] I. Tokarev, S. Minko, *Adv. Mater.* **2009**, *21*, 241.

[10] M. M. Orosco, C. Pacholski, M. J. Sailor, *Nat. Nanotechnol.* **2009**, *4*, 255.

[11] a) K. Nielsch, J. Choi, K. Schwirn, R. B. Wehrspohn, U. Gosele, *Nano Lett.* **2002**, *2*, 677; b) H. Masuda, K. Fukuda, *Science* **1995**, *268*, 1466; c) W. Lee, R. Ji, U. Gosele, K. Nielsch, *Nat. Mater.* **2006**, *5*, 741; d) P. Takmakov, I. Vlassiouk, S. Smirnov, *Analyst* **2006**, *131*, 1248; e) A. Thormann, N. Teuscher, M. Pfannmöller, U. Rothe, A. Heilmann, *Small* **2007**, *3*, 1032; f) K. E. La Flamme, K. C. Popat, L. Leoni, E. Markiewicz, T. J. La Tempa, B. B. Roman, C. A. Grimes, T. A. Desai, *Biomaterials* **2007**, *28*, 2638.

[12] S. B. Lee, D. T. Mitchell, L. Trofin, T. K. Nevanen, H. Soderlund, C. R. Martin, *Science* **2002**, *296*, 2198.

[13] M. Steinhart, R. B. Wehrspohn, U. Gosele, J. H. Wendorff, *Angew. Chem.* **2004**, *116*, 1356; *Angew. Chem. Int. Ed.* **2004**, *43*, 1334.

[14] C. R. Martin, P. Kohli, *Nat. Rev. Drug Discovery* **2003**, *2*, 29.

[15] C.-L. Feng, X. Zhong, M. Steinhart, A. M. Caminade, J. P. Majoral, W. Knoll, *Adv. Mater.* **2007**, *19*, 1933.

[16] S. J. Son, J. Reichel, B. He, M. Schuchman, S. B. Lee, *J. Am. Chem. Soc.* **2005**, *127*, 7316.

[17] P. Banerjee, I. Perez, L. Henn-Lecordier, S. B. Lee, G. W. Rubloff, *Nat. Nanotechnol.* **2009**, *4*, 292.

[18] C. R. Martin, *Science* **1994**, *266*, 1961.

[19] X. Wang, S. Smirnov, *ACS Nano* **2009**, *3*, 1004.

[20] a) D. Losic, D. Losic, Jr., *Langmuir* **2009**, *25*, 5426; b) D. Losic, M. Millo, D. Losic, Jr., *Small* **2009**, *5*, 1392; c) G. Meng, Y. J. Jung, A. Cao, R. Vajtai, P. M. Ajayan, *Proc. Natl. Acad. Sci. USA* **2005**, *102*, 7074; d) A. Y. Y. Ho, H. Gao, Y. C. Lam, I. Rodriguez, *Adv. Funct. Mater.* **2008**, *18*, 2057.

[21] a) V. Bala Murali, D. Brian, Y. Sukru, W. Nicholas, P. Ivan, B. Rashid, *Adv. Mater.* **2009**, *21*, 2771; b) T. Sano, N. Iguchi, K. Iida, T. Sakamoto, M. Baba, H. Kawaura, *Appl. Phys. Lett.* **2003**, *83*, 4438.

[22] C. Wu, T. Xu, W. Yang, *J. Membr. Sci.* **2003**, *224*, 117.

[23] T. Kyotani, W. Xu, Y. Yokoyama, J. Inahara, H. Touhara, A. Tomita, *J. Membr. Sci.* **2002**, *196*, 231.

[24] a) W. Shi, Y. Shen, D. Ge, M. Xue, H. Cao, S. Huang, J. Wang, G. Zhang, F. Zhang, *J. Membr. Sci.* **2008**, *325*, 801; b) C.-S. Chang, H.-S. Ni, S.-Y. Suen, W.-C. Tseng, H.-C. Chiu, C. P. Chou, *J. Membr. Sci.* **2008**, *311*, 336.

[25] a) W. Chen, J. H. Yuan, X. H. Xia, *Anal. Chem.* **2005**, *77*, 8102; b) A. Y. Ku, J. A. Ruud, T. A. Early, R. R. Corderman, *Langmuir* **2006**, *22*, 8277; c) E. D. Steinle, D. T. Mitchell, M. Wirtz, S. B. Lee, V. Y. Young, C. R. Martin, *Anal. Chem.* **2002**, *74*, 2416.

[26] a) T. M. McCleskey, D. S. Ehler, J. S. Young, D. R. Pesiri, G. D. Jarvinen, N. N. Sauer, *J. Membr. Sci.* **2002**, *210*, 273; b) F. Buyukserin, P. Kohli, M. O. Wirtz, C. R. Martin, *Small* **2007**, *3*, 266.

[27] a) D. M. Dotzauer, J. Dai, L. Sun, M. L. Bruening, *Nano Lett.* **2006**, *6*, 2268; b) L. Sun, J. Dai, G. L. Baker, M. L. Bruening, *Chem. Mater.* **2006**, *18*, 4033; c) S. U. Hong, R. Malaisamy, M. L. Bruening, *Langmuir* **2007**, *23*, 1716.

[28] D. Losic, M. A. Cole, B. Dollmann, K. Vasilev, H. J. Griesser, *Nanotechnology* **2008**, *19*, 245704.

[29] A. Yamaguchi, F. Uejo, T. Yoda, T. Uchida, Y. Tanamura, T. Yamashita, N. Teramae, *Nat. Mater.* **2004**, *3*, 337.

[30] Y. Wu, G. Cheng, K. Katsov, S. W. Sides, J. Wang, J. Tang, G. H. Fredrickson, M. Moskovits, G. D. Stucky, *Nat. Mater.* **2004**, *3*, 816.

[31] a) P.-S. Cheow, E. Z. C. Ting, M. Q. Tan, C.-S. Toh, *Electrochim. Acta* **2008**, *53*, 4669; b) B. T. T. Nguyen, E. Z. C. Ting, C.-S. Toh, *Bioinspiration Biomimetics* **2008**, *3*, 035008; c) W. Lee, R. Scholz, K. Nielsch, U. Gosele, *Angew. Chem.* **2005**, *117*, 6204; *Angew. Chem. Int. Ed.* **2005**, *44*, 6050; d) M. Lahav, T. Sehayek, A. Vaskevich, I. Rubinstein, *Angew. Chem.* **2003**, *115*, 5734; *Angew. Chem. Int. Ed.* **2003**, *42*, 5576; e) A. Johansson, J. Lu, J. O. Carlsson, M. Boman, *J. Appl. Phys.* **2004**, *96*, 5189.

[32] C. Z. Wang, E. Y. F, L. Z. Fan, Z. H. Wang, H. B. Liu, Y. L. Li, S. H. Yang, *Adv. Mater.* **2007**, *19*, 3677.

[33] A. Mutalib Md Jani, E. J. Anglin, S. J. P. McInnes, D. Losic, J. G. Shapter, N. H. Voelcker, *Chem. Commun.* **2009**, 3062.

[34] X. Wang, C. S. Ozkan, *Nano Lett.* **2008**, *8*, 398.

[35] A. Bernardos, E. Aznar, M. D. Marcos, R. Martinez-Manez, F. Sancenon, J. Soto, J. M. Barat, P. Amoros, *Angew. Chem.* **2009**, *121*, 5998; *Angew. Chem. Int. Ed.* **2009**, *48*, 5884.